The Lone Pair Electrons in Post-Transition Metal and Their Contribution to Optical Response*

WANG Jialong[1], ZHANG Ruixin[1], CUI Xiuhua[1], CHEN Zhaohui[2],
JING Qun[1†], DUAN Haiming[1]

(*1. Xinjiang Key Laboratory of Solid State Physics and Devices, School of Physical Science and Technology, Xinjiang University, Urumqi Xinjiang 830017, China; 2. Key Laboratory of Oil & Gas Fine Chemicals Ministry of Education & Xinjiang Uygur Autonomous Region, School of Chemical Engineering and Technology, Xinjiang University, Urumqi Xinjiang 830017, China*)

Abstract: The stereochemically active lone pairs around post-transition metal atoms play an important role in determining distorted lattice structure and optical response. The lone pair electrons are characterized by crystal orbitals, electron localization function (ELF) and partial density of states (PDOS). Birefringence is evaluated by means of a Born effective charge approach based on modern polarization theory. The origin of the different responses of birefringence and second-harmonic generation (SHG) is explored, as well as the effect of spin-orbit coupling (SOC) on the band structure and optical properties is explored. The study of this paper can help to deeply understand the lone pairs and their contribution to optical property.

Key words: lone pair electrons; birefringence; second-harmonic generation response; spin-orbit coupling; first-principles
DOI: 10.13568/j.cnki.651094.651316.2023.10.10.0003
CLC number: O734 **Document Code**: A **Article ID**: 2096-7675(2024)05-0579-012
引文格式：王嘉龙，张瑞鑫，崔秀花，陈兆慧，井群，段海明. 后过渡金属中的孤对电子及其对光学响应的贡献[J]. 新疆大学学报(自然科学版中英文)，2024，41(5)：579-590.
英文引文格式：WANG Jialong，ZHANG Ruixin，CUI Xiuhua，CHEN Zhaohui，JING Qun，DUAN Haiming. The lone pair electrons in post-transition metal and their contribution to optical response[J]. Journal of Xinjiang University(Natural Science Edition in Chinese and English)，2024，41(5)：579-590.

后过渡金属中的孤对电子及其对光学响应的贡献

王嘉龙[1]，张瑞鑫[1]，崔秀花[1]，陈兆慧[2]，井 群[1]，段海明[1]

(1. 新疆大学 物理科学与技术学院 新疆固体物理与器件自治区重点实验室，新疆 乌鲁木齐 830017；
2. 新疆大学 化工学院 石油天然气精细化工教育部和自治区重点实验室，新疆 乌鲁木齐 830017)

摘 要： 后过渡金属原子周围的立体化学活性孤对电子在决定扭曲晶格结构和光学响应方面起着重要作用. 孤对电子的表征方法包括晶体轨道、电子局部化函数和分波态密度. 通过基于现代偏振理论的 Born 有效电荷的方法对双折射进行评估，探究了双折射和二次谐波响应不同的起源，以及自旋轨道耦合对能带结构和光学性质的影响. 这有助于深入理解孤对电子及其对光学性质的贡献.

关键词： 孤对电子；双折射；倍频响应；自旋轨道耦合；第一性原理

0 Introduction

In the past five decades, China has made remarkable achievements in nonlinear optics (NLO), including anionic group

* **Received Date:** 2023-10-10
Foundation Item: This work was supported by the National Natural Science Foundation of the People's Republic of China "Mechanistic study of the influence of ns^2 cation intrinsic properties and coordination environment on birefringence and frequency doubling effects" (12264047), "The study of the mechanism of the influence of lead-oxygen polyhedra and their coordination environments on the gain of the frequency doubling effect" (11864040); Tianshan Talent Project of Xinjiang Uygur Autonomous Region of China "Design, synthesis and photofunctional study of novel rare earth phosphate materials" (2022TSYCJU0004).
Biography: WANG Jialong (2000—), male, master student, research fields: nonlinear optical crystal, E-mail: 107552200765@stu.xju.edu.cn.
† **Corresponding author:** JING Qun (1981—), male, associate professor, research fields: nonlinear optical crystal, E-mail: qunjing@xju.edu.cn.

theory[1−4], and a series of nonlinear optical materials with excellent performance[5−10], such as β-BaB_2O_4 (β-BBO)[11], LiB_3O_5 (LBO)[12], CsB_3O_5 (CBO)[13], $KBe_2BO_3F_2$ (KBBF)[14−15], et al.. Although the above crystals have been widely used in commercial applications, they still have their own shortcomings, and therefore the exploration of nonlinear optical crystals with better performance is still urgent.

In order to obtain nonlinear optical crystals with suitable birefringence and excellent SHG response, the general strategy is to enhance the performance by introducing various chromophores and thus enhancing the performance, including BO_3 and CO_3 groups with conjugated π-orbitals[8], post-transition metal cations containing ns^2np^0 lone pairs (Pb^{2+}, Sn^{2+}, Bi^{3+}, Sb^{3+})[16−17] and so on. For example, the powder SHG response of $Pb_2Ba_3(BO_3)_3Cl$[18] is 3.2×KDP, which is six times larger than its isomorphic $Ba_5(BO_3)_3Cl$. The SHG response of $Pb_2B_5O_9I$ is as high as 13.5×KDP[19]. In addition, the lone pairs were thought to be beneficial for enlarging birefringence[20]. For example, the birefringence of $PbCl_2$, $SbCl_3$, and α-SnF_2 are 0.046, 0.172, and 0.177@546 nm, respectively[21]. The first-principles investigation shows that the birefringence of $CsPbCO_3F$ is larger than that of $KSrCO_3F$[22]. The atomic contribution through Bader charge analysis and Born effective charge analysis show that the Pb^{2+} cations are beneficial to enlarge birefringence[23], and the enlargement has relation with the stereochemical activity of Pb^{2+} cations[24].

Recently, more complicated optical response was found in post-transition metal oxides/halides. For example, the SHG response of α-BiB_3O_6 is 3.2 pm/V (about 8.2×KDP)[25], which is larger than that of SbB_3O_6 (about 3.5×KDP)[26], while the birefringence of α-BiB_3O_6 is just 0.174@546 nm[27], which is smaller than that of SbB_3O_6 (0.290@546 nm). The birefringence of $Sn_2B_5O_9Cl$ is 0.168@546 nm, larger than its isomorphic $Ba_2B_5O_9Cl$ and $Pb_2B_5O_9Cl$ whose values are 0.010@546 nm[28] and 0.067@546 nm[29], respectively. While the SHG response of $Sn_2B_5O_9Cl$ is only 0.5×KDP[29], which is much smaller than that of its isomorphic $Ba_2B_5O_9Cl$ (about 3.5×KDP)[30] and $Pb_2B_5O_9Cl$ (about 4×KDP)[31]. The birefringence and SHG of $Sn_2B_5O_9Br$ is 0.439@546 nm and 2.4×KDP (still smaller than $Ba_2B_5O_9Br$ as well as $Pb_2B_5O_9Br$)[29,32−33]. In a word, a so-called "different optical response" was found in these post-transition metal borates. That is those borates containing $5s^25p^0$ post-transition metal atoms own relatively larger birefringence and relatively smaller SHG response comparison with those containing $6s^26p^0$ atoms. Similar different optical response was also found in fluoroborates. For example, the different optical responses of $PbB_2O_3F_2$, and $SnB_2O_3F_2$. First-principles investigation shows that the Sn atoms own relatively stronger stereochemically activity[34], and the birefringence of $PbB_2O_3F_2$ and $SnB_2O_3F_2$ are 0.017 and 0.130, respectively[35]. However, the SHG response of these compounds are 13×KDP and 4×KDP, respectively[34].

To deeply understand the origination about the so-called "different optical response" in these post-transition metal oxides/halides, lots of efforts have been made, including the revised model firstly proposed by Walsh et al.[16], modern polarization theory, SOC, and kinds of analysis based on the first-principles results including ELF, PDOS, real space atom-cutting method (RSAC), and so on. In this paper, we would give some comments about these methods, and try to dig out the role played by lone pairs in the optical response. The results show that in affecting birefringence and SHG response: Lone pairs in post-transition metal atoms play an important role in determining the distorted lattice structure, birefringence and SHG response. The lone pairs of electrons at the Fermi level are the main contributors to the birefringence, whereas the extended covalent bonds at the top of the valence band (including the lone pairs of electrons near the Fermi level) are the contributors to the SHG response, which leads to the so-called difference in the birefringence and SHG response after the substitution of post-transition metal cations. In terms of characterization techniques for lone pairs of electrons: Lone pairs can be represented by crystal orbitals near the Fermi level, ELF and PDOS. It is noted that the ELF should be calculated using the full-electron or full-potential projected augmented wave (PAW) method, whereas after accounting for the SOC effect, the post-transition metal-containing compounds suffer from a downward shift of the conduction band as well as band splitting of the conduction band at a particular k-point, which leads to a decrease of the band gap, an enhancement of the birefringence and the SHG response. We hope this paper could help to understand the lone pairs and their contribution to birefringence and SHG response and help to design and synthesis kinds of nonlinear optical compounds.

1 Revised Lone Pair Model

1.1 Walsh's Model

The lone pair is a valence shell orbital but not a covalent bond. It plays an important role in determining the molecular geometry. The distorted geometry of moleculars like H_2O, NH_3, and so on can be explained by the valence shell electron

pair repulsion theory (VSEPR) proposed by Sidgwick et al.[36], and Gillespie et al.[37]. The stereochemically active lone pair owns asymmetric electron distribution leading to Jahn-Teller geometry distortion and enlargement of optical response, so it cannot be formed by pure symmetric 5s or 6s orbitals. Orgel[38] argues that the stereochemically active lone pair can be formed by hybridization of the outmost s and p orbitals becauses, and p orbitals have different spatial symmetry. The classical model proposed by Orgel is successful in explaining the distorted crystal geometries containing stereochemically active lone pairs. However, there are still some difficulties in explaining why some compounds that require electronic configuration to form stereochemically active lone pairs do not exhibit such pronounced lattice distortions[16]. For example, stereochemically activity can be found in typical metal oxide compounds PbO[39−40] and SnO[41−42], but PbS and SnTe[16] have symmetric rock salt structures (shown in Fig 1).

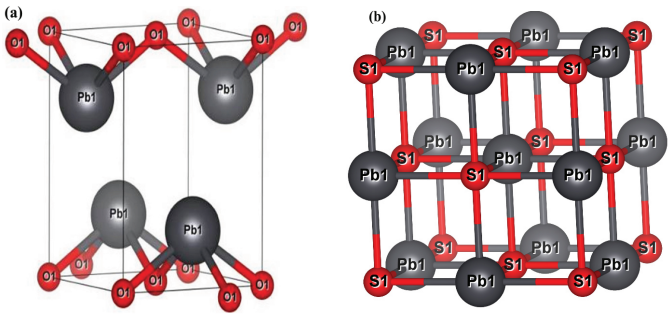

Fig 1 The geometry of (a) lead yellow PbO and (b) rock salt PbS

After detailed investigation the electronic structures of a series of post-transition metal compounds, Walsh et al.[41] proposed a revised model about stereochemistry of post-transition metal oxides comparison with classical lone pair model. Herein take SnX (X = O, S, Se, Te) as an example. The revised model believes that the Sn-s orbitals are not chemical inserts, it can hybridize with X-p orbitals to form (Sn s-X p) bonding states and (Sn s-X p)* antibonding states (shown in Fig 2). Both (Sn s-X p) bonding states and (Sn s-X p)* antibonding states are located at bottom of valence band. And then in the distorted structures the unoccupied Sn p states can hybridize with the (Sn s-X p)* antibonding states, resulting in a stabilization of occupied electronic states nearby the Fermi level. According to the revised model, one can utilize ELF, the crystal orbitals nearby the Fermi level and PDOS to check out the stereochemically active lone pairs around post-transition metal atoms.

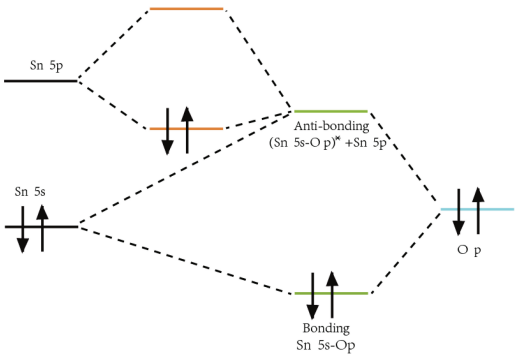

Fig 2 Illustration about atomic orbital interaction leading to form stereochemically active lone pairs

Walsh et al.[41] also pointed out that the relative energies of the cation s state, and anion p states are crucial in the formation of stereochemically active lone pairs. The closer they are, the stronger the interaction and more (cationic s-anionic p)*-cationic p occupied states are present[43], leading to stronger stereochemically active lone pairs and greater lattice distortion. We have recalculated the atomic orbital energies using the Gaussian09 code[44]. The atomic orbital energies were obtained at CAM-B3LYP/Def2-TZVPP level. The obtained atomic orbital energies are shown in Fig 3. According to the revised model proposed by Walsh et al.[41], the stabilization order of lone pairs follows Sn > Pb > Sb > Bi, and for given post-transition metal like PbX_2 (X = F, Cl, Br, I) the strength of stereochemically active can be explained by the interaction between Pb and X atoms as ΔE_{s-p} own the sequence of Pb-Cl < Pb-Br < Pb-I.

1.2 Diagram about Lone Pairs

As described above, one can utilize the crystal orbitals, PDOS, ELF, et al. to represent the lone pairs. In this paper, we have repeated the electronic structures of a series of post-transition metal oxides/halides using the first-principles method implemented in CASTEP code[45]. These post-transition metal oxides/halides are the binary metal halides MX_2 (M = Sn, Pb; X = Cl, Br, I)[46], the binary metal oxides MO, BiB_3O_6, $SbB_3O_6^{[47]}$, MPO_3F, $M_3(PO_4)_2$[48], $MB_2O_3F_2$[35] (M = Sn, Pb, Ba),

$CsPbCO_3F$, $RbCdCO_3F$, $RbSrCO_3F$, $KSrCO_3F$[49−50], $CsSnCl_3$, $CsSnI_3$, $CsPbCl_3$, and $CsPbI_3$[46], and so on. The obtained crystal orbitals, the ELF and PDOS are shown in Figs 4~6 and Figs S1~S6 (Download from https://xjdz.cbpt.cnki.net/portal/journal/portal/client/download/xjdz_54253c13-816a-4cda-85b4-048f7444fa78?t=%E4%B8%8B%E8%BD%BD%E4%B8%AD%E5%BF%83).

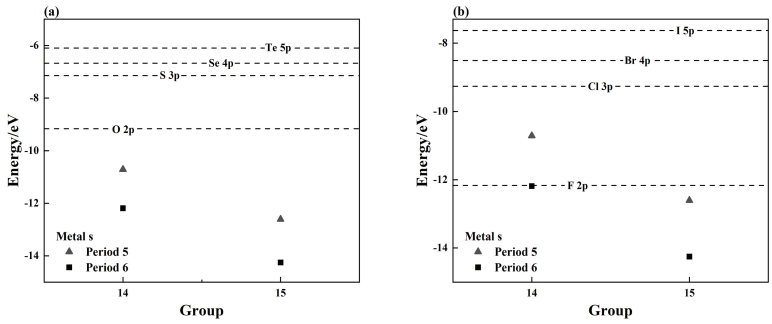

Fig 3 The atomic orbital energies of elements of (a) the sixth and (b) the seventh main groups and post-transition metal elements

The obtained crystal orbital at the Fermi level is shown in Fig 4. As shown in Fig 4, there are semilunar or first-quarter-moon like asymmetric electron distribution around the Pb^{2+} and Sn^{2+} cations, which are the asymmetric lone pairs. On the same scale, the asymmetric electronic distribution around Sn^{2+} is larger than Pb^{2+}, indicating Sn^{2+} has stronger stereochemically active lone pairs. Noting that, as shown in Fig 9 in reference [35], stereochemically active lone pairs are found not only the one at the Fermi level, but also other lower states, which are -1.54, -0.81, -0.56 below the Fermi level. Unlike lead and antimony cations, the asymmetric lone pair was not found around Ba^{2+} cations.

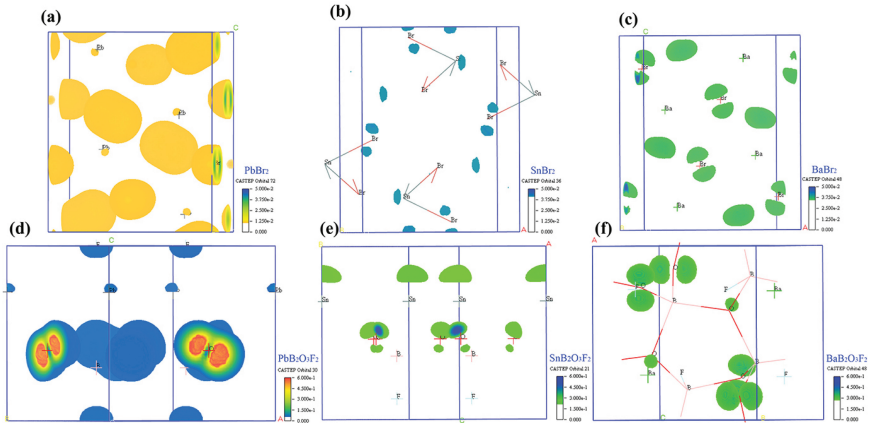

Fig 4 The crystal orbitals nearby the Fermi level of (a~c) MBr_2 and (d~f) $MB_2O_3F_2$, M = Pb, Sn, Ba

ELF[51] is a useful tool to investigate the atomic interaction and nonbonding lone pairs[52−53]. The values ranging in [0.5, 1] are ascribed to bonding and nonbonding localized electron pairs, and smaller values in [0, 0.5] could be delocalized electrons. ELF was usually utilized to visualize stereochemically active ns^2np^0 lone pair. For example, Ju et al.[54] have investigated the ELF of Bi_2ZnTiO_6 using the GGA functional and full-potential PAW method implemented in VASP code. The lobe shaped electrons were found around bismuth. As shown in Fig 5, the asymmetric ELF was found around Pb^{2+} and Sn^{2+} cations, indicating the stereochemically active lone pairs.

We would give some comments about the method that can distinguish the lone pairs in post-transition metal oxides/halides. Orbitals nearby the Fermi level and ELF are often used to distinguish the lone pairs because they can give more intuitive pictures of asymmetric lone pairs. While there are still some drawbacks of these two methods. For orbitals nearby the Fermi level, it is uneasy to distinguish the lone pairs if the stereochemically active is weak. The ELF was developed for all electron descriptions, while the CASTEP calculations are performed using the valence electrons, so it might be less meaningful. According to the definition of ELF introduced by Becke et al.[51], the ELF has value in the range of [0, 1]. The value of ELF close to 1 correspond to well-localized electrons or lone pairs of electrons. But the ELF values from CASTEP code do not span the full range of [0, 1], so extremely localized or delocalized electrons and lone pairs cannot be well described. Hence we suggest using both ELF and PDOS to identify the lone pairs of electrons.

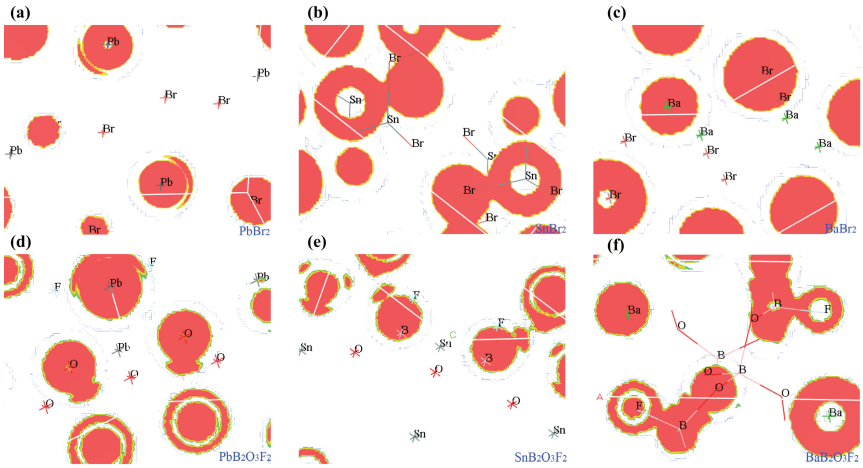

Fig 5 The ELF of (a~c) MBr_2 and (d~f) $MB_2O_3F_2$, M = Pb, Sn, Ba

Let's check the obtained PDOS of MBr_2 (M = Pb, Sn, Ba) and $MB_2O_3F_2$ (M = Pb, Sn, Ba) shown in Fig 6. Take $SnBr_2$ for example. At the valence band, the (Sn s-Br p) states are located nearby -6 eV, and the expanded (Sn s-Br p)* states are located at the energy region (-4, -1) eV. The hybrid (Sn s-Br p)*-Sn p states are found nearby the Fermi level. According to the revised model proposed by Walsh et al.[41], the hybrid (Sn s-Br p)*-Sn p should be the occupied lone pairs states. Similar conclusion can also be found in $PbBr_2$ compound (shown in Fig 6) and other post-transition metal oxides/halides (shown in Figs S1~S6). Noting that the PDOS nearby the Fermi level in $SnBr_2$ is stronger than $PbBr_2$, indicating the antimony owns stronger stereochemically active lone pairs than lead atoms. As for the PDOS of $MB_2O_3F_2$ compounds shown in Fig 6, the occupied lone pairs (Sn 5s-O 2p)*-Sn 5p hybrid states and (Pb 6s-O 2p)*-Pb 6p hybrid states are found nearby the Fermi level in $SnB_2O_3F_2$ and $PbB_2O_3F_2$, respectively, and the Sn^{2+} peak is larger (1.06) than Pb^{2+} peak (0.18) according to integral calculation results. Nonbonding states of oxygen atoms were found in nearby Fermi level of $BaB_2O_3F_2$ compounds.

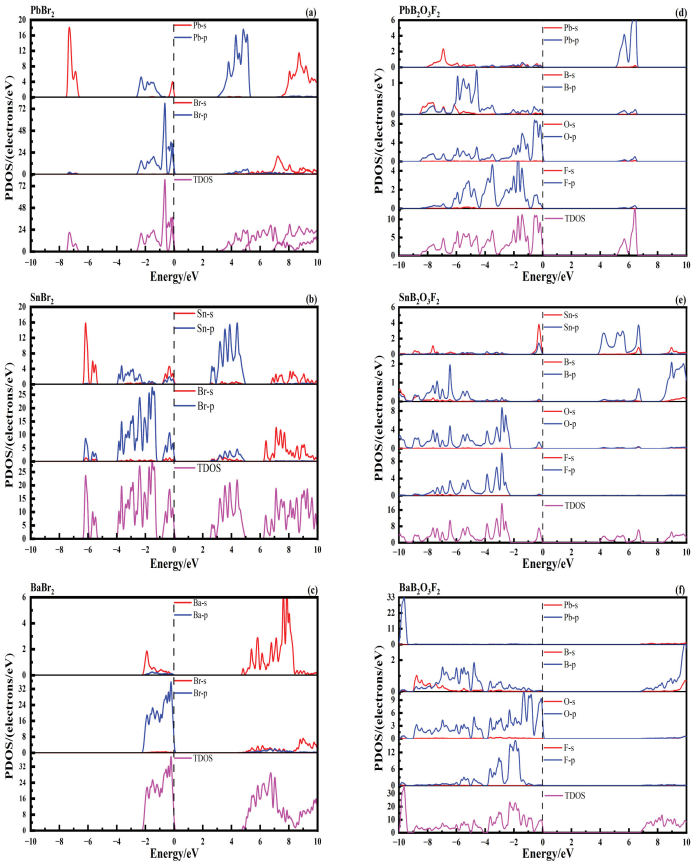

Fig 6 The PDOS of (a~c) MBr_2 and (d~f) $MB_2O_3F_2$, M = Pb, Sn, Ba

2 Methods Evaluating the Birefringence

2.1 Birefringence Obtained by OptaDOS Code

As a fundamental and important optical parameter, birefringence plays an important role in the application of the optical communication devices[55], NLO materials[56], and so on. For instance, an NLO material should own moderate birefringence to meet the phase-matching condition to get noticeable SHG output[57]. Hence the relative small birefringence limits the widely application of the LiB_3O_5[58], and the very small birefringence (about 0.004 3~0.002 1@212.9~1 064.4 nm) makes the SrB_4O_7 uneasy to meet the phase-matching conditions[59].

Due to the difficulty in synthesizing the large sized crystals which can be used to measure the refractive indices, the anisotropic birefringence was merely reported except for some very famous birefringent materials. To evaluate the application of the nonlinear optical materials, lots of efforts have been made to investigate the refractive indices and especially the anisotropic birefringence using various methods[60–61], among which the first-principles method is widely used. Using CASTEP code implemented in Materials Studio, it is easy to get refractive indices along different dielectric axis with orthorhombic, tetragonal, cubic, trigonal, and hexagonal crystal system[57,62–64], but it is difficult to get refractive indices for the monoclinic or triclinic materials such as $Ca_5(BO_3)_3F$[65–66] and BiB_3O_6[67]. As described elsewhere[65–66], for these monoclinic materials only one dielectric axis is found to be superposed on one crystallographic axis, the other two are not related to any specific crystallographic directions[68]. On the other hand, it is more convenient to get the refractive indices along different dielectric axis not only with orthorhombic, tetragonal cubic, trigonal, and hexagonal crystal system but also for monoclinic or triclinic materials using the OptaDOS code[69–71] based on the electronic structure obtained by CASTEP code. After the electronic structures were obtained, the imaginary part of the dielectric constant ε_2 can be obtained by

$$\varepsilon_2 = \frac{2e^2\pi}{\Omega\varepsilon_0}\sum_{\kappa,v,c}|<\varphi_\kappa^c|u\cdot r|\varphi_\kappa^v>|^2\delta(E_\kappa^c - E_\kappa^v - E).$$

In which Ω is the volume of the elemental cell, v and c represent the valence and conduction bands, respectively, and u is the vector defining the polarization of the electric field of the incident light. The real part of dielectric constant $\varepsilon_1$was then obtained via a Kramers-Kronig transform. In practical calculation, when the grid summation was performed, the δ functions should be replaced by normalized functions with nonzero width such as Gaussian-type functions[71]. While it is uneasy to estimate the level spacing, hence it is difficult to get suitable Gaussian width which may lead to error. Yates et al.[71] point out that a good adaptive broadening scheme for k-space integration may lead to quite well results. The refractive index n was obtained by

$$n^2 = \frac{1}{2}\left(\sqrt{\varepsilon_1^2+\varepsilon_2^2}+\varepsilon_1^2\right).$$

Reliable values of birefringence were obtained using the OptaDOS code and compared with experimental values as shown in Tables 1 and 2.

2.2 Born Effective Charge

During the past decades, lots of methods have been used to dig out the atomic contribution to the total birefringence, including RSAC method[78], Born effective charge, and so on. They are already many literatures and comments about the RSAC methods, so we would just give some comments about Born effective charge based on modern polarization theory[79]. The modern polarization theory defines the spontaneous polarization of a periodic solid and provides a route to calculate the electronic structures and polarization through the Berry phase[80]. The Born effective charge is defined as

$$q_{ij}^{\text{Born}} = \frac{\pi}{e}\frac{\delta P_i}{\delta d_j},$$

in which the δP_i is the change in polarization along the displacement direction δd_i. Using the Born effective charge, one can deduce the change of polarization along with the ionic displacement. It is well known that the birefringence has relation with the anisotropic polarization, so one can utilize the Born effective charge to investigate the atomic contribution to total birefringence.

Take $CsPbCO_3F$ for example. The $CsPbCO_3F$ compound crystallizes into a hexagonal crystal system, hence the polarization of n_o and n_e are in xy plane, and along z axis, respectively. As described in Table 2 in reference [79], the obtained

refractive indices own the sequence as $n_o > n_e$, so if the obtained atomic Born effective charge $q_{xx}(q_{yy})$ is larger than q_{zz}, one can deduce that the atoms give positive contribution to the birefringence. Otherwise, if obtained atomic Born effective charge owns the sequence as $q_{xx}(q_{yy}) < q_{zz}$, it gives negative contribution to the total birefringence. Hence the lead atoms give positive contribution to the birefringence. Furthermore, from the difference of Born effective charges along the dielectric axis (marked as Δq), one can also deduce the level of the atomic contribution. For example, the Δq of Pb atoms in KPb_2CO_3F (about 0.98) is larger than that in $CsPbCO_3F$ (about 0.59), which makes the former have relatively larger birefringence than the latter. By the way, unlike the case of $ABCO_3F$, many compounds have off-diagonal tensor elements because the Born effective charge is a two-order tensor.

Table 1 The obtained refractive indices and birefringence of a series of borates (uniaxial crystals) without concerning scissors operator

Crystals Type	Borates	Experimental Values				Calculation Values			
		λ (nm)	n_o	n_e	Δn	n_o	n_e	Δn	error
Uniaxial Crystals	α−BaB_2O_4[72]	1 064.0	–	–	0.116	1.751	1.641	0.110	-5.17%
	$BaAlBO_3F_2$[73]	1 064.0	1.619	1.578	0.041	1.718	1.677	0.041	0.00%
		580.0	1.631	1.587	0.044	1.732	1.690	0.042	-4.55%
	β−BaB_2O_4[73]	1 014.0	1.656	1.543	0.113	1.767	1.648	0.119	5.31%
		546.1	1.674	1.555	0.119	1.790	1.665	0.125	5.04%
	$KBe_2BO_3F_2$[73]	656.3	1.477	1.400	0.077	1.528	1.464	0.064	16.88%
		546.1	1.479	1.403	0.076	1.532	1.468	0.064	-15.79%
	$CsLiB_6O_{10}$[73]	1 064.0	1.484	1.434	0.050	1.567	0.505	0.062	24.00%
		590.0	1.494	1.442	0.052	1.578	1.514	0.064	23.08%
	$Li_2B_4O_7$[73]	1 013.9	1.599	1.544	0.055	1.672	1.613	0.059	7.27%
		546.1	1.613	1.556	0.057	1.687	1.625	0.062	8.77%
	$CsBe_2BO_3F_2$[74]	1 014.0	1.502	1.443	0.059	1.580	1.526	0.054	-8.47%
		546.1	1.515	1.450	0.065	1.591	1.536	0.055	15.38%
	$RbBe_2BO_3F_2$[75]	1 014.0	1.479	1.407	0.072	1.544	1.486	0.058	-19.44%
		644.0	1.485	1.411	0.074	1.550	1.491	0.059	-20.27%
	$Ba_2Na_3(B_3O_6)_2F$[76]	1 014.0	1.610	1.512	0.098	1.714	1.613	0.101	3.06%
		546.1	1.626	1.522	0.104	1.735	1.628	0.107	2.88%

Table 2 The obtained refractive indices and birefringence of a series of borates (biaxial crystals) without concerning scissors operator

Crystals Type	Borates	Experimental Values					Calculation Values				
		λ (nm)	n_1	n_2	n_3	Δn	n_1	n_2	n_3	Δn	error
Biaxial Crystals	BiB_3O_6[73]	1 079.5	1.757	1.783	1.916	0.159	2.024	1.885	1.870	0.154	-3.14%
		539.8	1.787	1.819	1.961	0.174	2.079	1.931	1.910	0.169	-2.87%
	LiB_3O_5[73]	1 064.0	1.565	1.591	1.605	0.040	1.696	1.659	1.647	0.049	22.50%
		546.1	1.578	1.606	1.621	0.043	1.713	1.674	1.661	0.052	20.93%
	$Ca_5(BO_3)_3F$[77]	1 064.0	1.594	1.630	1.645	0.051	1.770	1.756	1.716	0.054	5.88%
		546.1	1.609	1.649	1.663	0.054	1.795	1.781	1.738	0.057	5.56%

3 Different Response of Birefringence and SHG

As described above, the $6s^26p^0$ lone pairs have different response of birefringence and SHG comparison with $5s^25p^0$ lone pairs. For example, the obtained birefringence of $MB_2O_3F_2$ compounds is $BaB_2O_3F_2$ (0.014 pm/V) < $PbB_2O_3F_2$ (0.017 pm/V) < $SnB_2O_3F_2$ (0.130 pm/V), and the obtained effective SHG response are $BaB_2O_3F_2$ (0.45 pm/V) < $SnB_2O_3F_2$ (0.73 pm/V) < $PbB_2O_3F_2$ (4.30 pm/V), respectively. As described above, the antimony atoms own stronger stereochemically active lone pairs than lead atoms. So, the former should own stronger birefringence and SHG response than the latter, how can the latter have stronger SHG response than the former?

To deeply understand the origination about the different response of birefringence and SHG response, the RSAC method and band resolved SHG response method were introduced. During the calculation, the cutting radius of Ba, Sn, Pb, B, O

and F are set as 1.5, 1.2, 1.4, 0.8, 1.1 and 1.2 Å, respectively. The obtained results show that the BOF groups give little contribution to birefringence, and main contribution to the birefringence comes from the SnO/PbO and PbF groups. As for SHG response, main contribution also comes from the SnO/PbO groups, and the BOF's contribution is almost negligible.

The contribution from each atom and each state are further investigated using the band resolved SHG response. The obtained band resolved SHG response are shown in Fig 7. As shown in Fig 7, these states nearby the Fermi level give main contribution to the SHG response. And the states in region I of $SnB_2O_3F_2$ are larger than that of $PbB_2O_3F_2$, which may have relation with the fact that $SnB_2O_3F_2$ own stronger stereochemical active lone pairs locating nearby Fermi level. The states in region II also give contribution to the SHG response of $PbB_2O_3F_2$. The virtual hole (VH) process gives negative contribution, resulting in decreased SHG response of $SnB_2O_3F_2$. The VH progress give similar contribution like VE progress to SHG response of $PbB_2O_3F_2$. In a word, the stereochemical active lone pairs nearby the Fermi level make $SnB_2O_3F_2$ own enhanced birefringence comparison with $PbB_2O_3F_2$ and $BaB_2O_3F_2$, while not only the lone pairs shown in region I but also the expanded hybrid cation-oxygen states in region I and region II (even in deep energy region) give contribution to the SHG response, leading to enhanced SHG response comparison with $SnB_2O_3F_2$ and $BaB_2O_3F_2$.

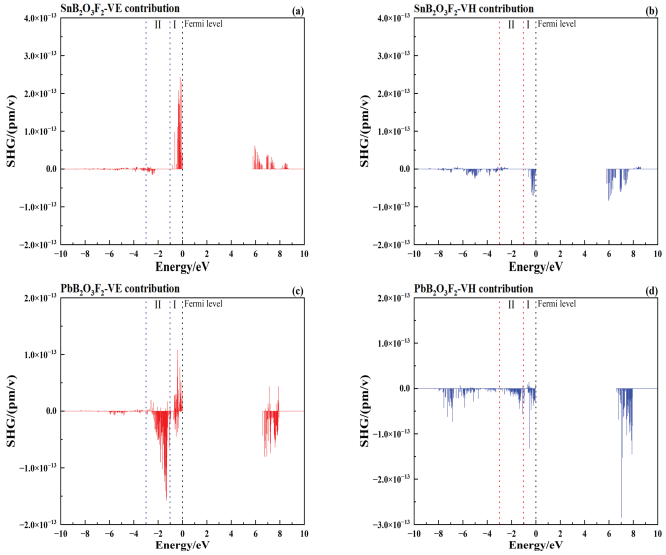

Fig 7 The band contributions to the total SHG responses of (a~b) $SnB_2O_3F_2$ and (c~d) $PbB_2O_3F_2$

4 The SOC Effect

In an asymmetric crystal, electronic energy bands are split by SOC[81]. When an electron with momentum p moves in a magnetic field, its Lorentz force is

$$F = -ep \times \frac{B}{m},$$

and its Zeeman energy should be

$$\mu\sigma \times B.$$

And when this electron moves in an electronic field E, like the electronic field produced by ion core (containing atomic nucleus and inner-shell electrons), the ion core would produce a magnetic field

$$B = \frac{\hbar}{m_e c^2} L \frac{\mathrm{d}V(r)}{r\mathrm{d}r},$$

in which the electronic field $E = -\nabla V r$. The SOC should be

$$H_{\mathrm{soc}} = \frac{Z^4 e^2 \hbar^2}{4\pi m_e^2 c^2 \varepsilon_0 a_0^3 n^3 l(l+1)(2l+1)} L \cdot S = \lambda L \cdot S,$$

in which Z is atomic number. Hence one can deduce that the post-transition metal atoms should have relatively large SOC.

Although SOC has been utilized to investigate the spin transistor, spin-orbit qubits, spin-orbit torque, Dirac materials, and so on, there is still rare report about the nonlinear optical response induced by SOC. In 2017, Narsimha et al.[82] have

reported the role of SOC on the nonlinear optical response of $CsPbCO_3F$. The results show a considerable reduction of bandgap after SOC was taken into consideration. The obtained bandgaps with SOC are 3.03 (PBE), 2.94 (PBEsol) and 4.45 (TB-mBJ), while the bandgap without SOC are 3.59 (PBE), 3.48 (PBEsol), and 5.58 (TB-mBJ), respectively. The reduction of bandgap comes from the downshift of Pb-p states at the bottom of conduction band, whereas no changes of valence band nearby the Fermi level were observed. The enhanced birefringence was found after SOC was applied. The obtained birefringence with SOC is 0.105 69, and the obtained birefringence without SOC is 0.104 89. Jiang et al.[83] have investigated the role of large Rashba SOC in SHG of BIBO. We found a smaller bandgap coming from band splitting and band repulsion after the SOC was turned on. The obtained bandgap with SOC is 4.8 eV (HSE06), and the bandgap without SOC is 5.1 eV (HSE06). The bandgap with SOC is more accurately comparison with experimental values (4.7 eV). Furthermore, after considering the SOC, the obtained SHG response are in better agreement with experimental values comparison with the case without SOC. And major Rashba splitting was found at the A point in the k_x-k_y plane (shown in Fig 1(a) in reference [83]).

5 Conclusion

In a word, lone pairs in post-transition metal atoms play an important role in determining distorted lattice structure, birefringence and SHG response. The stability of stereochemically active lone pairs is determined by the difference of atomic orbital energies of cationic s and anionic p states. The lone pairs can be represented using the crystal orbitals nearby Fermi level, the ELF, and PDOS. Noting that ELF should be calculated using the full electron or full-potential PAW method. The atomic contribution to birefringence and SHG response can be evaluated using the Born effective charge based on modern polarization theory, RSAC method and so on. Lone pair electrons at Fermi level give main contribute to birefringence and expanded covalent bonds at the top of valence band including lone pairs nearby the Fermi level give contribution to the SHG response, which leads to the so-called different response of birefringence and SHG response after post-transition metal cations substitution. The SOC coming from post-transition metal leads to the downshift of conduction band and band splitting of conduction band at special k points, and then the reduction of bandgap and enhanced birefringence and SHG response.

References:

[1] CHEN C T. An ionic grouping theory of the electro-optical and non-linear optical effects of crystals (I): A theoretical calculation of electro-optical and second optical harmonic coefficients of Barium titanate crystals based on a deformed oxygen-octahedra[J]. Acta Physica Sinica, 1976, 25(2): 146-161.

[2] CHEN C T. An ionic grouping theory of the electro-optical and non-linear optical effects of crystals (II): A theoretical calculation of the second harmonic optical coefficients of the lithium iodate crystal based on a highly deformed oxygen-octahedra model I[J]. Acta Physica Sinica, 1977, 26(2): 124-132.

[3] CHEN C T. An ionic grouping theory of the electro-optical and non-linear optical effects of crystals (III): A theoretical calculation of the electro-optical and optical second harmonic coefficients for $LiNbO_3$, $LiTaO_3$, $KNbO_3$, and BNN crystals based on a defo[J]. Acta Physica Sinica, 1977, 26(6): 486-499.

[4] CHEN C T. An ionic grouping theory of the electro-optical and non-linear optical effects of crystals (IV): The calculation of linear optical susceptibilities in crystals of the perovskite and the tungsten bronze structure types[J]. Acta Physica Sinica, 1978, 27(1): 41-46.

[5] CHEN C T, LI T R, WU Y, et al. Nonlinear optical borate crystals: Principals and applications[J]. Discrete Mathematics, 2012, 26(2): 43-50.

[6] WANG W K, MEI D J, LIANG F, et al. Inherent laws between tetrahedral arrangement pattern and optical performance in tetrahedron-based mid-infrared nonlinear optical materials[J]. Coordination Chemistry Reviews, 2020, 421: 213444.

[7] LIU X M, GONG P F, YANG Y, et al. Nitrate nonlinear optical crystals: A survey on structure-performance relationships[J]. Coordination Chemistry Reviews, 2019, 400: 213045.

[8] MUTAILIPU M, POEPPELMEIER K R, PAN S L. Borates: A rich source for optical materials[J]. Chemical Reviews, 2021, 121(3): 1130-1202.

[9] MUTAILIPU M, PAN S L. Emergent deep-ultraviolet nonlinear optical candidates[J]. Angewandte Chemie International Edition, 2020, 59(46): 20302-20317.

[10] GAO L, HUANG J B, GUO S R, et al. Structure-property survey and computer-assisted screening of mid-infrared nonlinear optical chalcohalides[J]. Coordination Chemistry Reviews, 2020, 421: 213379.

[11] CHEN C T, WU B C, JIANG A D, et al. A new-type ultraviolet SHG crystal: β-BaB_2O_4[J]. Scientia Sinica (Series B), 1985, 28(3): 235-243.

[12] CHEN C T, WU Y C, JIANG A D, et al. New nonlinear-optical crystal: LiB_3O_5[J]. Journal of the Optical Society of America B, 1989, 6(4): 616-621.

[13] WU Y C, SASAKI T, NAKAI S D, et al. CsB_3O_5: A new nonlinear optical crystal[J]. Applied Physics Letters, 1993, 62(21): 2614-2615.

[14] MEI L, HUANG X, WANG Y Q, et al. Crystal structure of $KBe_2BO_3F_2$[J]. Zeitschrift Für Kristallographie - Crystalline Materials, 1995, 210(2): 93-95.

[15] CHEN C T, XU Z Y, DENG D Q, et al. The vacuum ultraviolet phase-matching characteristics of nonlinear optical $KBe_2BO_3F_2$ crystal[J]. Applied Physics Letters, 1996, 68(21): 2930-2932.

[16] WALSH A , PAYNE D J , EGDELL R G , et al. Stereochemistry of post-transition metal oxides : Revision of the classical lone pair model[J]. Chemical Society Reviews , 2011 , 40(9) : 4455-4463.
[17] PAYNE D J , EGDELL R G , WALSH A , et al. Electronic origins of structural distortions in post-transition metal oxides : Experimental and theoretical evidence for a revision of the lone pair model[J]. Physical Review Letters , 2006 , 96(15) : 157403.
[18] DONG X Y , JING Q , SHI Y J , et al. $Pb_2Ba_3(BO_3)_3Cl$: A material with large SHG enhancement activated by Pb-chelated BO_3 groups[J]. Journal of the American Chemical Society , 2015 , 137(29) : 9417-9422.
[19] HUANG Y Z , WU L M , WU X T , et al. $Pb_2B_5O_9I$: An iodide borate with strong second harmonic generation[J]. Journal of the American Chemical Society , 2010 , 132(37) : 12788-12789.
[20] HAN S J , MUTAILIPU M , TUDI A , et al. $PbB_5O_7F_3$: A high-performing short-wavelength nonlinear optical material[J]. Chemistry of Materials , 2020 , 32(5) : 2172-2179.
[21] YANG Y , QIU Y , GONG P F , et al. Lone-pair enhanced birefringence in an alkaline-earth metal tin(II) phosphate $BaSn_2(PO_4)_2$[J]. Chemistry - A European Journal , 2019 , 25(22) : 5648-5651.
[22] GUO J Y , TUDI A , HAN S J , et al. α-SnF_2 : A UV birefringent material with large birefringence and easy crystal growth[J]. Angewandte Chemie International Edition , 2021 , 60(7) : 3540-3544.
[23] LIN C S , ZHOU A Y , CHENG W D , et al. Atom-resolved analysis of birefringence of nonlinear optical crystals by Bader charge integration[J]. The Journal of Physical Chemistry C , 2019 , 123(51) : 31183-31189.
[24] JING Q , YANG Z H , PAN S L , et al. Contribution of lone-pairs to birefringence affected by the Pb(II) coordination environment : A DFT investigation[J]. Physical Chemistry Chemical Physics , 2015 , 17(34) : 21968-21973.
[25] HELLWIG H , LIEBERTZ J , BOHATÝ L. Exceptional large nonlinear optical coefficients in the monoclinic bismuth borate BiB_3O_6 (BIBO)[J]. Solid State Communications , 1998 , 109(4) : 249-251.
[26] LIU Y C , LIU X M , LIU S , et al. An unprecedented antimony(III) borate with strong linear and nonlinear optical responses[J]. Angewandte Chemie International Edition , 2020 , 59(20) : 7793-7796.
[27] HELLWIG H , LIEBERTZ J , BOHATÝ L. Linear optical properties of the monoclinic bismuth borate BiB_3O_6[J]. Journal of Applied Physics , 2000 , 88(1) : 240-244.
[28] GUO J Y , TUDI A , HAN S J , et al. $Sn_2B_5O_9Cl$: A material with large birefringence enhancement activated prepared via alkaline-earth-metal substitution by tin[J]. Angewandte Chemie International Edition , 2019 , 58(49) : 17675-17678.
[29] GUO J Y , CHENG S C , HAN S J , et al. $Sn_2B_5O_9Br$ as an outstanding bifunctional material with strong second-harmonic generation effect and large birefringence[J]. Advanced Optical Materials , 2021 , 9(5) : 2001734.
[30] 陈兆慧 , 潘世烈 , 赵文武 , 等. 非线性光学晶体 $Ba_2B_5O_9Cl$ 的合成、晶体生长及性能的研究[J]. 人工晶体学报 , 2011 , 40(6) : 1394-1398.
CHEN Z H , PAN S L , ZHAO W W , et al. Study on synthesis , crystal growth and properties of nonlinear optical crystal $Ba_2B_5O_9Cl$[J]. Journal of Synthetic Crystals , 2011 , 40(6) : 1394-1398. (in Chinese)
[31] CHEN Z H , PAN S L , YANG Z H , et al. $Pb_2B_5O_9Cl$: A chloride borate with second harmonic generation effect[J]. Journal of Materials Science , 2013 , 48(6) : 2590-2596.
[32] EGOROVA B V , OLENEV A V , BERDONOSOV P S , et al. Lead-strontium borate halides with hilgardite-type structure and their SHG properties[J]. Journal of Solid State Chemistry , 2008 , 181(8) : 1891-1898.
[33] PLACHINDA P A , DOLGIKH V A , STEFANOVICH S Y , et al. Nonlinear-optical susceptibility of hilgardite-like borates $M_2B_5O_9X$ (M= Pb, Ca, Sr, Ba; X= Cl, Br)[J]. Solid State Sciences , 2005 , 7(10) : 1194-1200.
[34] LUO M , LIANG F , SONG Y X , et al. Rational design of the first lead/tin fluorooxoborates $MB_2O_3F_2$ (M =Pb, Sn) , containing flexible two-dimensional $[B_6O_{12}F_6]^{\infty}$ single layers with widely divergent second harmonic generation effects[J]. Journal of the American Chemical Society , 2018 , 140(22) : 6814-6817.
[35] SHI X R , JING Q , CHEN Z H , et al. Different mechanism of response of asymmetric lone pair electrons around ns^2 cations to birefringence and second harmonic generation[J]. Journal of Applied Physics , 2020 , 128(11) : 113104.
[36] SIDGWICK N V , POWELL H M. Bakerian Lecture : Stereochemical types and valency groups[J]. Proceedings of the Royal Society of London Series A , 1940 , 176(965) : 153-180.
[37] GILLESPIE R J , NYHOLM R S. Inorganic stereochemistry[J]. Quarterly Reviews , Chemical Society , 1957 , 11(4) : 339-380.
[38] ORGEL L E. The stereochemistry of B subgroup metals. Part II. The inert pair[J]. Journal of the Chemical Society , 1959(0) : 3815-3819.
[39] WATSON G W , PARKER S C , KRESSE G. *Ab initio* calculation of the origin of the distortion of α-PbO[J]. Physical Review B , 1999 , 59(13) : 8481-8486.
[40] WATSON G W , PARKER S C. Origin of the lone pair of α-PbO from density functional theory calculations[J]. The Journal of Physical Chemistry B , 1999 , 103(8) : 1258-1262.
[41] WALSH A , WATSON G W. Electronic structures of rocksalt , litharge , and herzenbergite SnO by density functional theory[J]. Physical Review B , 2004 , 70(23) : 235114.
[42] WATSON G W. The origin of the electron distribution in SnO[J]. Journal of Chemical Physics , 2001 , 114(2) : 758-763.
[43] ZHU Y , WU H , CUI X. Stereochemical activity of lone pair electrons in a class of metal halides and its effect on birefringence[J]. Journal of Physics B : Atomic , Molecular and Optical Physics , 2023 , 40(6) : 158-168.
[44] FRISCH A. Gaussian 09W reference[M]. Wallingford : Gaussian , Inc , 2009.
[45] CLARK S J , SEGALL M D , PICKARD C J , et al. First principles methods using CASTEP[J]. Zeitschrift Für Kristallographie - Crystalline Materials , 2005 , 220(5/6) : 567-570.
[46] WANG K , JING Q , WAN Z Z , et al. Different mechanism of stereochemical activity and birefringence in post-transition metal halides : A

first-principles investigation[J]. Journal of Solid State Chemistry, 2021, 297(1): 122038.
[47] SHI X R, JING Q, LEE M H, et al. A first-principle investigate about the different response of birefringence and SHG from AB_3O_6 (A=Bi, Sb) compounds[J]. Chemical Physics Letters, 2022, 786: 139188.
[48] QIAN Y Y, JING Q, DUAN H M, et al. First-principles study of the influence of lone pair electrons and molecular groups on the birefringence of phosphate and fluorophosphate[J]. Physica B: Condensed Matter, 2022, 630: 413676.
[49] JING Q, YANG G, CHEN Z H, et al. A joint strategy to evaluate the microscopic origin of the second-harmonic-generation response in nonpolar $ABCO_3F$ compounds[J]. Inorganic Chemistry, 2018, 57(3): 1251-1258.
[50] JING Q, YANG G, HOU J, et al. Positive and negative contribution to birefringence in a family of carbonates: A Born effective charges analysis[J]. Journal of Solid State Chemistry, 2016, 244: 69-74.
[51] BECKE A D, EDGECOMBE K E. A simple measure of electron localization in atomic and molecular systems[J]. The Journal of Chemical Physics, 1990, 92(9): 5397-5403.
[52] GIBBS G V, COX D F, BOISENJRM B, et al. The electron localization function: A tool for locating favorable proton docking sites in the silica polymorphs[J]. Physics and Chemistry of Minerals, 2003, 30(5): 305-316.
[53] SAVIN A, NESPER R, WENGERT S, et al. ELF: The electron localization function[J]. Angewandte Chemie International Edition in English, 1997, 36(17): 1808-1832.
[54] JU S, GUO G Y. First-principles study of crystal structure, electronic structure, and second-harmonic generation in a polar double perovskite Bi_2ZnTiO_6[J]. The Journal of Chemical Physics, 2008, 129(19): 194704.
[55] ZHANG H, ZHANG M, PAN S L, et al. $Na_3Ba_2(B_3O_6)_2F$: Next generation of deep-ultraviolet birefringent materials[J]. Crystal Growth & Design, 2015, 15(1): 523-529.
[56] XIA Y N, CHEN C T, TANG D Y, et al. New nonlinear optical crystals for UV and VUV harmonic generation[J]. Advanced Materials, 1995, 7(1): 79-81.
[57] LIN Z S, JIANG X X, KANG L, et al. First-principles materials applications and design of nonlinear optical crystals[J]. Journal of Physics D: Applied Physics, 2014, 47(25): 253001.
[58] CHEN C T, WU Y C, JIANG A D, et al. New nonlinear-optical crystal: LiB_3O_5[J]. Journal of the Optical Society of America B, 1989, 6(4): 616-621.
[59] OSELEDCHIK Y S, PROSVIRNIN A L, PISAREVSKIY A I, et al. New nonlinear optical crystals: Strontium and lead tetraborates[J]. Optical Materials, 1995, 4(6): 669-674.
[60] SHANNON R D, FISCHER R X. Empirical electronic polarizabilities in oxides, hydroxides, oxyfluorides, and oxychlorides[J]. Physical Review B, 2006, 73(23): 235111.
[61] QIN F L, LI R K. Predicting refractive indices of the borate optical crystals[J]. Journal of Crystal Growth, 2011, 318(1): 642-644.
[62] LIN Z S, KANG L, ZHENG T, et al. Strategy for the optical property studies in ultraviolet nonlinear optical crystals from density functional theory[J]. Computational Materials Science, 2012, 60: 99-104.
[63] NAHERM I, NAQIBS H. A comprehensive study of the thermophysical and optoelectronic properties of Nb_2P_5 via *ab-initio* technique[J]. Results in Physics, 2021, 28: 104623.
[64] BIAN Q, YANG Z H, DONG L Y, et al. First principle assisted prediction of the birefringence values of functional inorganic borate materials[J]. The Journal of Physical Chemistry C, 2014, 118(44): 25651-25657.
[65] XU K, LOISEAU P, AKA G, et al. Nonlinear optical properties of $Ca_5(BO_3)_3F$ crystal[J]. Optics Express, 2008, 16(22): 17735-17744.
[66] HU C L, XU X, SUN C F, et al. Electronic structures and optical properties of $Ca_5(BO_3)_3F$: A systematical first-principles study[J]. Journal of Physics: Condensed Matter, 2011, 23(39): 395501.
[67] BOHATY L, OCHROMBEL R, LIEBERTZ J, et al. Linear electrooptic effect of the monoclinic polar bismuth triborate, BiB_3O_6[J]. Crystal Research and Technology, 2017, 52(1): 1600250.
[68] JING Q, DONG X Y, YANG Z H, et al. The interaction between cations and anionic groups inducing SHG enhancement in a series of apatite-like crystals: A first-principles study[J]. Journal of Solid State Chemistry, 2014, 219: 138-142.
[69] MORRIS A J, NICHOLLS R J, PICKARD C J, et al. OptaDOS: A tool for obtaining density of states, core-level and optical spectra from electronic structure codes[J]. Computer Physics Communications, 2014, 185(5): 1477-1485.
[70] NICHOLLS R J, MORRIS A J, PICKARD C J, et al. OptaDOS: A new tool for EELS calculations[J]. Journal of Physics: Conference Series, 2012, 371: 012062.
[71] YATES J R, WANG X J, VANDERBILT D, et al. Spectral and Fermi surface properties from Wannier interpolation[J]. Physical Review B, 2007, 75(19): 195121.
[72] ZHOU G Q, XU J, CHEN X D, et al. Growth and spectrum of a novel birefringent α-BaB_2O_4 crystal[J]. Journal of Crystal Growth, 1998, 191(3): 517-519.
[73] NIKOGOSYAN D N. Nonlinear optical crystals: A complete survey[M]. Berlin: Springer, 2005.
[74] HUANG H W, CHEN C T, WANG X Y, et al. Ultraviolet nonlinear optical crystal: $CsBe_2BO_3F_2$[J]. Journal of the Optical Society of America B, 2011, 28(9): 2186-2190.
[75] ZHAI N X, WANG L R, LIU L J, et al. Measurement of thermal refractive index coefficients of nonlinear optical crystal $RbBe_2BO_3F_2$[J]. Optical Materials, 2013, 36(2): 333-336.
[76] WANG X, XIA M J, LI R K. A promising birefringent crystal $Ba_2Na_3(B_3O_6)_2F$[J]. Optical Materials, 2014, 38: 6-9.
[77] XU K, LOISEAU P, AKA G, et al. A new promising nonlinear optical crystal for ultraviolet light generation: $Ca_5(BO_3)_3F$[J]. Crystal Growth & Design, 2009, 9(5): 2235-2239.
[78] LIN J, LEE M H, LIU Z, et al. Mechanism for linear and nonlinear optical effects in β-BaB_2O_4 crystals[J]. Physical Review B, 1999, 60(13): 13380.

[79] SPALDIN N A. A beginner′s guide to the modern theory of polarization[J]. Journal of Solid State Chemistry, 2012, 195: 2-10.
[80] WANG C, YU R, KRAKAUER H. Polarization dependence of Born effective charge and dielectric constant in $KNbO_3$[J]. Physical Review B, 1996, 54: 11161.
[81] MANCHON A, KOO H C, NITTA J, et al. New perspectives for Rashba spin-orbit coupling[J]. Nature Materials, 2015, 14(9): 871-882.
[82] NARSIMHA R E, VAITHEESWARAN G, RESHAK A H, et al. Role of spin-orbit interaction on the nonlinear optical response of $CsPbCO_3F$ using DFT[J]. Physical Chemistry Chemical Physics, 2017, 19(46): 31255-31266.
[83] JIANG X, YE L T, WU X Q, et al. Role of large Rashba spin-orbit coupling in second-order nonlinear optical effects of polar BiB_3O_6[J]. Physical Review B, 2022, 106(19): 195126.

责任编辑：张自强 刘敏

(上接第 578 页)

Problem 1 $D_n^{sl}(Q_n) = \lceil\lceil(2^n-2)/(n-1)\rceil\rceil + 1$ for $n \geq 3$?

We have determined the spanning wide diameter of generalized Petersen graph $P(n,1)$. It has been studied the spanning connectivity of $P(n,2)$ and $P(n,3)$ respectively in [13] and [20-21]. The same question is also interesting for $P(n,2)$ and $P(n,3)$.

Problem 2 What are the spanning wide diameters of generalized Petersen graphs $P(n,2)$ and $P(n,3)$?

References:

[1] FAUDREE R J. Some strong variations of connectivity[J]. Combinatorics, 1993, 1: 125-144.
[2] FLANDRIN E, LI H. Mengerian properties, hamiltonicity, and claw-free graphs[J]. Networks, 1994, 24(3): 177-183.
[3] HSU D F. On container width and length in graphs, groups, and networks[J]. IEICE Transactions on Fundamentals of Electronics, Communications and Computer Sciences, 1994, 77(4): 668-680.
[4] FRANK HSU D, UCZAK T. On the k-diameter of k-regular k-connected graphs[J]. Discrete Mathematics, 1994, 133(1/2/3): 291-296.
[5] HSU D F, LYU Y D. A graph-theoretical study of transmission delay and fault tolerance[J]. International Journal of Mini & Microcomputers, 1994, 16: 35-42.
[6] MA M J, WEST D B, XU J M. The vulnerability of the diameter of the enhanced hypercubes[J]. Theoretical Computer Science, 2017, 694: 60-65.
[7] QI H, ZHU X D. The wide-diameter of $Z_{n,K}$[J]. Discrete Applied Mathematics, 2017, 219: 193-201.
[8] QI H, ZHU X D. The fault-diameter and wide-diameter of twisted hypercubes[J]. Discrete Applied Mathematics, 2018, 235: 154-160.
[9] LIN C K, HUANG H M, HSU L H. On the spanning connectivity of graphs[J]. Discrete Mathematics, 2007, 307(2): 285-289.
[10] HSU L H, LIN C K. Graph theory and interconnection networks[M]. Boca Raton: CRC Press, 2008.
[11] LIN C K, HUANG H M, HSU D F, et al. On the spanning w-wide diameter of the star graph[J]. Networks, 2006, 48(4): 235-249.
[12] CHANG C H, LIN C K, HUANG H M, et al. The super laceability of the hypercubes[J]. Information Processing Letters, 2004, 92(1): 15-21.
[13] ALBERT M, ALDRED R E L, HOLTON D, et al. On 3^*-connected graphs[J]. The Australasian Journal of Combinatorics, 2001, 24: 193-207.
[14] HARARY F, HAYES J P. Edge fault tolerance in graphs[J]. Networks, 1993, 23(2): 135-142.
[15] HARARY F, HAYES J P. Node fault tolerance in graphs[J]. Networks, 1996, 27(1): 19-23.
[16] SABIR E, VUMAR E. Spanning connectivity of the power of a graph and Hamilton-connected index of a graph[J]. Graphs and Combinatorics, 2014, 30(6): 1551-1563.
[17] KAO S S, HSU H C, HSU L H. Globally bi-3^*-connected graphs[J]. Discrete Mathematics, 2009, 309(8): 1931-1946.
[18] CHANG C H, SUN C M, HUANG H M, et al. On the equitable k^*-laceability of hypercubes[J]. Journal of Combinatorial Optimization, 2007, 14(2): 349-364.
[19] KOBEISSI M, MOLLARD M. Disjoint cycles and spanning graphs of hypercubes[J]. Discrete Mathematics, 2004, 288(1/2/3): 73-87.
[20] WANG J J, HSU L H. On the spanning connectivity of the generalized Petersen graphs $P(n,3)$[J]. Discrete Mathematics, 2018, 341(3): 672-690.
[21] EMINJAN S, SHANG H, MENG J X. On the spanning connectivity of graphs: A survey[J]. Journal of Xinjiang University(Natural Science Edition), 2018, 35(4): 379-388.

责任编辑：张自强 刘敏